arXiv:2007.03198v1 [cs.LG] 7 Jul 2020

# Regional Image Perturbation Reduces $L_p$ Norms of Adversarial Examples While Maintaining Model-to-model Transferability

**Utku Ozbulak** [*1 2] **Jonathan Peck** [*3 4] **Wesley De Neve** [1 2] **Bart Goossens** [5]
**Yvan Saeys** [3 4] **Arnout Van Messem** [3 2]

## Abstract

Regional adversarial attacks often rely on complicated methods for generating adversarial perturbations, making it hard to compare their efficacy against well-known attacks. In this study, we show that effective regional perturbations can be generated without resorting to complex methods. We develop a very simple regional adversarial perturbation attack method using cross-entropy sign, one of the most commonly used losses in adversarial machine learning. Our experiments on ImageNet with multiple models reveal that, on average, 76% of the generated adversarial examples maintain model-to-model transferability when the perturbation is applied to local image regions. Depending on the selected region, these localized adversarial examples require significantly less $L_p$ norm distortion (for $p \in \{0, 2, \infty\}$) compared to their non-local counterparts. These localized attacks therefore have the potential to undermine defenses that claim robustness under the aforementioned norms.

## 1. Introduction

Recent advancements in the field of machine learning (ML) — more specifically, in deep learning (DL) — have substantially increased the adoption rate of automated systems in everyday life (Krizhevsky et al., 2012; He et al., 2016; Xie et al., 2017). However, since their inception, these systems have been criticized for their lack of *interpretability*: it is often difficult or impossible to know precisely *why* an ML model produces a specific response for a given input, yet such information is highly relevant in many settings (Ghorbani et al., 2017; Kindermans et al., 2017). One

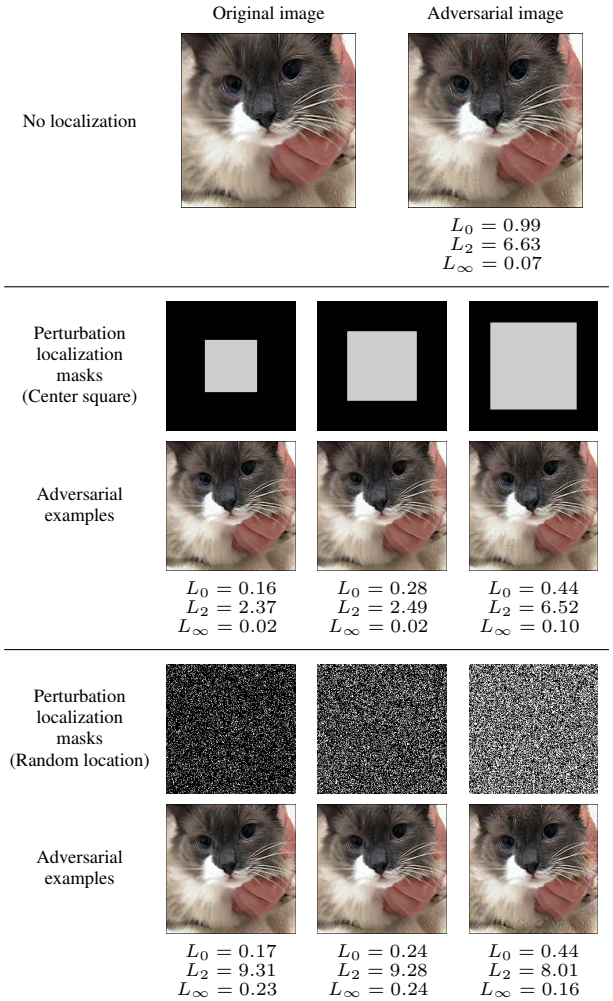


*Figure 1.* (Top) An input image and its adversarial counterpart created with IFGS. (Center and bottom) Perturbation localization grids illustrated with black-gray images and adversarial examples generated by IFGS when the perturbation is only applied to the grey areas in the localization grids. $L_p$ norms of the perturbation are provided under each image. All of the adversarial examples were generated using AlexNet and successfully transfer to ResNet-50.

[*]Equal contribution [1]Department of Electronics and Information Systems, Ghent University, Ghent, Belgium [2]Center for Biotech Data Science, Ghent University Global Campus, Incheon, Republic of Korea [3]Department of Applied Mathematics, Computer Science and Statistics, Ghent University, Ghent, Belgium [4]Data Mining and Modeling for Biomedicine, VIB Inflammation Research Center, Ghent, Belgium [5]Department of Telecommunications and Information Processing, Ghent University - imec, Ghent, Belgium. Correspondence to: Utku Ozbulak <utku.ozbulak@ugent.be>.

Presented at the ICML 2020 Workshop on Uncertainty and Robustness in Deep Learning. Copyright 2020 by the author(s).

manifestation of this shortcoming of current ML theory to understand DL models is the phenomenon of *adversarial examples* (Szegedy et al., 2013), which has recently received much attention in the research community. Adversarial examples are data points specifically crafted by an adversary in order to force machine learning models into making mistakes. Often, these artificial examples are visually indistinguishable from natural data points, making it almost impossible for humans to detect them and calling into question the generalization ability of deep neural networks (DNN) (Schmidt et al., 2018; Ilyas et al., 2019).

Formally, adversarial examples are usually defined as follows (Szegedy et al., 2013; Madry et al., 2017). Given an ML model $f$ and an input $\boldsymbol{X}$, an adversarial example $\tilde{\boldsymbol{X}}$ satisfies (1) $\|\boldsymbol{X} - \tilde{\boldsymbol{X}}\|_p \leq \varepsilon$ for some chosen $L_p$ norm and perturbation budget $\varepsilon > 0$ and (2) $f(\boldsymbol{X}) \neq f(\tilde{\boldsymbol{X}})$. In other words, the perturbed input $\tilde{\boldsymbol{X}}$ must be "close" to the original input $\boldsymbol{X}$ as measured by an $L_p$ norm and the classifier $f$ must output different labels for $\boldsymbol{X}$ and $\tilde{\boldsymbol{X}}$. However, for sufficiently small values of $\varepsilon$, the two inputs are indistinguishable and should belong to the same class. Hence, the existence of adversarial examples for very small perturbation budgets indicates a failure of DL models to accurately capture the data manifold. Interestingly, depending on the attack used, adversarial examples can be highly *transferable*: an adversarial sample $\tilde{\boldsymbol{X}}$ that fools a certain classifier $f$ can also fool completely different classifiers trained for the same task (Papernot et al., 2016; Cheng et al., 2019). This so-called *transferability*, i.e., the degree to which an adversarial sample can fool other models, is a popular metric for assessing the effectiveness of a particular attack.

Through the generations of research in computer vision it was established that certain regions of images are more important for the identification of an object of interest than others (Moravec, 1981; Schmid & Mohr, 1997; Lowe, 2004; Sun et al., 2014; Springenberg et al., 2014; Selvaraju et al., 2016). As such, research on localized adversarial attacks also shows that adversarial perturbation applied to these *important* regions may change the prediction faster and with less $L_p$ perturbation than attacks that apply the perturbation to the entire image (Su et al., 2017; Karmon et al., 2018; Xu et al., 2018; Zajac et al., 2019). However, analyses to prevent adversarial examples often do not evaluate robustness against such regional attacks. Adversarial defenses are often studied exclusively against well-understood attacks such as FGS (Goodfellow et al., 2014), JSMA (Papernot et al., 2015), IFGS (Kurakin et al., 2016), Carlini & Wagner's Attack (Carlini & Wagner, 2016), PGD (Madry et al., 2017), and BPDA (Athalye et al., 2018), where these attacks apply their perturbations to the entire image based on the magnitude of the loss gradient for each pixel and according to the $L_p$ norm constraints they set. We believe this lack of evaluation against regional attacks is because (1) regional attacks are often studied in permissive white-box settings which do not represent real-world scenarios and (2) the proposed attacks usually come with a completely new and complicated way of generating adversarial examples, thus making it not straightforward to apply these attacks to different datasets, especially not locally, as opposed to well-understood attacks.

In this work, we show that so-called "global" adversarial attacks can be easily modified to become localized attacks. As such, different from previous research efforts on localized perturbation, our study does not propose a novel attack. Instead, we introduce a general method for localizing the perturbations generated by existing non-localized attacks. We achieve this by multiplying the original perturbations by a simple binary mask (as shown in Figure 1), restricting the perturbation to specific image regions. We analyze both the transferability and the $L_p$ norm properties of the crafted adversarial examples, finding that the localized examples are about as effective as the examples generated by the original attacks (in terms of transferability), and with the localized versions often requiring significantly less $L_p$ distortion. The implementation of the proposed method is publicly available[1].

The finding that we can significantly reduce the required $L_p$ distortion while maintaining similar levels of effectiveness potentially undermines many existing defenses — certified or not — since these usually guarantee robustness against specific $L_p$ perturbation budgets (Wong & Kolter, 2017; Croce et al., 2018; Andriushchenko & Hein, 2019; Ghiasi et al., 2020). Reducing the required distortion attacks below such thresholds could render these defenses ineffective.

## 2. Framework

**Data** Adversarial examples are mainly studied on MNIST (LeCun et al., 1998), CIFAR (Krizhevsky & Hinton, 2009), or ImageNet (Russakovsky et al., 2015). However, as the field of adversarial machine learning evolved, due to shortcomings in terms of color channels and image sizes, the MNIST and CIFAR datasets are not deemed to be suitable for studies that represent real-world scenarios where adversarial examples pose a threat (Carlini & Wagner, 2017). Following this observation, we use images taken from the test set of the ImageNet dataset in order to generate adversarial examples.

**Models** Although convolutional architectures were already used in the work of LeCun et al. (1998), it was the success of AlexNet in 2012 that popularized DNN architectures (Krizhevsky et al., 2012). Recent research in the field of adversarial robustness also revealed AlexNet to be one

[1] github.com/utkuozbulak/regional-adversarial-perturbation

of the more robust architectures (Su et al., 2018). Following the success of AlexNet, VGG (Simonyan & Zisserman, 2014) architectures were proposed with smaller convolutional kernel sizes. Thanks to their simple architecture, VGG architectures are still popular today in many computer vision approaches. In order to overcome problems with vanishing gradients in deep architectures, He et al. (2016) proposed ResNet architectures, introducing the usage of residual layers. These residual architectures were later expanded upon and are currently some of the most frequently used architectures for solving a variety of problems in the field of deep learning (Xie et al., 2017; Hara et al., 2018). Given the history of the aforementioned architectures in the field of adversarial machine learning, as well as in other deep learning areas, we opted for the use of AlexNet, VGG-16, and ResNet-50 in our experiments.

## 3. Experimental Setup

**Generating adversarial examples** Carlini & Wagner (2017) demonstrated the fragility of adversarial examples generated by single-step attacks and argued that iterative attacks should be used for evaluating novel defenses. Iterative attacks calculate and add perturbation to the input iteratively according to the rule

$$\boldsymbol{X}_{n+1} = \boldsymbol{X}_n + \boldsymbol{P}_n \,, \tag{1}$$

where $\boldsymbol{X}_n$ and $\boldsymbol{P}_n$ represent the input and the perturbation generated at the $n$th iteration, respectively. In this study we generate the perturbation as follows:

$$\boldsymbol{P}_n = \alpha \,\mathrm{sign}\big(\nabla_x J(g(\theta, \boldsymbol{X}_n)_c)\big) \,, \tag{2}$$

where $\nabla_x J(g(\theta, \boldsymbol{X}_n)_c)$ represents the gradient with respect to $\boldsymbol{X}$ obtained with the cross-entropy loss ($J$) when targeting the class $c$. We use $\alpha = 0.004$ as the perturbation multiplier which approximately corresponds to changing the pixel values of images by $1/255$ at each iteration and perform this attack for $250$ iterations. Typically, adversarial attacks such as FGS, IFGS, and PGD enforce a constraint on the magnitude $\|\boldsymbol{X} - \tilde{\boldsymbol{X}}\|_p$ of the perturbation. However, in order to make a valid comparison between adversarial examples in terms of $L_0$, $L_2$, and $L_\infty$ norms, we only enforce a discretization constraint, thus ensuring that the produced adversarial examples can be represented as valid images (i.e., the pixel values of $\tilde{\boldsymbol{X}}$ lie within the range $[0, 1]$, as can be expected from regular images).

**Localizing adversarial perturbation** In a previous research effort (Ozbulak et al., 2019), we successfully used the Hadamard product to select target pixels for generating adversarial examples in the context of semantic segmentation (Ozbulak et al., 2019). In order to localize the perturbation to selected regions, we employ a similar approach in this research effort, making use of

$$\boldsymbol{X}_{n+1} = \boldsymbol{X}_n + \boldsymbol{P}_n \odot \boldsymbol{L} \,, \tag{3}$$

where $\boldsymbol{L}$ is a *localization mask*, i.e., a binary tensor of the same shape as the input. In this tensor, regions where the perturbation needs to be applied are set to $1$ while the remainder is set to $0$.

**Perturbation regions** In this study, we evaluate the use of three different perturbation regions, each with three different settings. These regions are (1) randomly selected pixels, (2) center square pixels, and (3) outer frame pixels. For (1), we randomly select $\{45\%, 28\%, 17\%\}$ of all pixels, where these percentages approximately correspond to a center square with a side length of $\{90, 120, 150\}$ pixels and an outer frame with a width of $\{20, 34, 58\}$ pixels, respectively. Thus, the number of selected pixels for all regions in each of the three different settings is virtually the same. Visual examples of the localization masks are provided in Figure 3 in Appendix A.

**Calculating $L_p$ distances** We calculate $L_p$ distances ($p = 0, 2, \infty$) between genuine images and their adversarial counterparts, similar the calculations in Papernot et al. (2015) and Carlini & Wagner (2017). A detailed description of these calculations for our settings is also provided in Appendix A.

## 4. Experiments

We first analyze model-to-model transferability (also called black-box transferability) for adversarial examples with localized perturbation. For each model-to-model pair, we generate $2,000$ adversarial examples that transfer from the source model to the target model. Using the same initial images as these adversarial examples do, we now apply perturbation to nine different regions (i.e., three regions, with each region coming with three different settings). In Figure 2, we present the percentage of adversarial examples that transfer from model to model when localized perturbation is applied, as opposed to performing the adversarial attack without any localization constraints. We see that a large portion of adversarial examples maintains model-to-model transferability when perturbation is applied to local regions.

For the adversarial examples that maintain model-to-model transferability, Table 1 provides exhaustive details on the mean and standard deviation of the $L_2$ and $L_\infty$ properties of the produced adversarial examples. $L_0$ norms are omitted from this table because adversarial examples with regional perturbation almost always have reduced mean $L_0$ norms (Figure 5 and Table 2 in Appendix B). Adversarial perturbation applied to the center square of an image reduces the mean $L_2$ norm while it increases the mean $L_\infty$ norm. However, with additional experiments, we discover that $43\%$ of the individual adversarial examples with localized perturbation have lower $L_\infty$ distances than their non-locally

Target Model

| Source Model | AlexNet | VGG-16 | ResNet-50 |
|---|---|---|---|
| AlexNet | 100% | 73% | 66% |
| VGG-16 | 60% | 100% | 56% |
| ResNet-50 | 52% | 59% | 100% |

(a) 17% of pixels selected

Target Model

| Source Model | AlexNet | VGG-16 | ResNet-50 |
|---|---|---|---|
| AlexNet | 100% | 76% | 67% |
| VGG-16 | 70% | 100% | 63% |
| ResNet-50 | 67% | 65% | 100% |

(b) 28% of pixels selected

Target Model

| Source Model | AlexNet | VGG-16 | ResNet-50 |
|---|---|---|---|
| AlexNet | 100% | 78% | 75% |
| VGG-16 | 83% | 100% | 75% |
| ResNet-50 | 78% | 77% | 100% |

(c) 45% of pixels selected

*Figure 2.* Percentage of adversarial examples with localized perturbation that transfer from source model (generated from) to target model (tested against) when 17%, 28%, and 45% of pixels are selected, respectively (combining all 3 localization approaches).

*Table 1.* Mean (standard deviation) $L_{\{2,\infty\}}$ distances calculated between genuine images and their adversarial counterparts, with the adversarial counterparts created by localization of perturbation (see the first column). Adversarial examples are created from the source models listed in the first row and transfer to the target models listed in the second row.

| Localization | Source: | AlexNet | | | | VGG-16 | | | | ResNet-50 | | | |
|---|---|---|---|---|---|---|---|---|---|---|---|---|---|
| | Target: | VGG-16 | | ResNet-50 | | AlexNet | | ResNet-50 | | AlexNet | | VGG-16 | |
| | Norm: | $L_2$ | $L_\infty$ | $L_2$ | $L_\infty$ | $L_2$ | $L_\infty$ | $L_2$ | $L_\infty$ | $L_2$ | $L_\infty$ | $L_2$ | $L_\infty$ |
| No Localization | | 7.35 (5.37) | 0.07 (0.08) | 6.39 (4.50) | 0.05 (0.06) | 6.91 (4.17) | 0.07 (0.05) | 3.62 (3.16) | 0.02 (0.04) | 6.79 (4.31) | 0.07 (0.06) | 3.76 (2.20) | 0.02 (0.02) |
| Center | 90px | 6.55 (4.36) | 0.15 (0.14) | 5.33 (3.52) | 0.11 (0.10) | 4.01 (2.64) | 0.10 (0.09) | 3.41 (2.77) | 0.09 (0.10) | 3.54 (2.54) | 0.09 (0.09) | 2.79 (2.23) | 0.06 (0.07) |
| | 120px | 6.47 (4.48) | 0.11 (0.11) | 6.30 (4.45) | 0.10 (0.11) | 5.01 (2.99) | 0.10 (0.08) | 3.68 (3.05) | 0.06 (0.07) | 4.50 (2.93) | 0.09 (0.08) | 3.70 (3.09) | 0.06 (0.08) |
| | 150px | 6.80 (4.48) | 0.10 (0.10) | 6.46 (4.33) | 0.09 (0.09) | 6.71 (3.79) | 0.11 (0.08) | 3.92 (3.07) | 0.05 (0.06) | 6.64 (3.90) | 0.11 (0.08) | 4.65 (3.54) | 0.07 (0.07) |
| Frame | 20px | 9.86 (8.37) | 0.18 (0.20) | 10.1 (7.94) | 0.20 (0.21) | 6.07 (3.74) | 0.16 (0.14) | 4.64 (3.61) | 0.12 (0.15) | 4.77 (2.88) | 0.13 (0.12) | 4.32 (2.90) | 0.11 (0.11) |
| | 34px | 8.92 (6.60) | 0.13 (0.13) | 8.63 (6.52) | 0.13 (0.14) | 6.71 (4.04) | 0.15 (0.12) | 4.50 (2.96) | 0.08 (0.08) | 5.68 (3.25) | 0.12 (0.09) | 4.85 (3.44) | 0.10 (0.10) |
| | 58px | 8.44 (5.72) | 0.12 (0.13) | 7.23 (4.94) | 0.09 (0.11) | 7.79 (4.17) | 0.14 (0.09) | 5.44 (3.89) | 0.08 (0.09) | 7.02 (3.90) | 0.12 (0.09) | 5.78 (3.79) | 0.09 (0.08) |
| Random | 17% | 8.11 (5.63) | 0.15 (0.16) | 7.41 (4.63) | 0.13 (0.14) | 5.20 (3.14) | 0.13 (0.11) | 4.43 (3.30) | 0.10 (0.12) | 4.59 (2.65) | 0.10 (0.09) | 3.81 (2.92) | 0.08 (0.09) |
| | 28% | 6.82 (4.99) | 0.10 (0.12) | 7.51 (4.54) | 0.11 (0.11) | 5.97 (3.55) | 0.12 (0.10) | 4.29 (2.91) | 0.07 (0.07) | 5.50 (3.14) | 0.11 (0.09) | 4.35 (3.02) | 0.07 (0.08) |
| | 45% | 7.42 (4.80) | 0.10 (0.11) | 6.76 (4.20) | 0.09 (0.09) | 7.21 (3.98) | 0.12 (0.09) | 4.61 (3.41) | 0.06 (0.07) | 7.39 (4.03) | 0.12 (0.08) | 5.04 (3.53) | 0.07 (0.07) |

perturbed counterparts, showing that localized perturbation nevertheless reduces the $L_\infty$ norm for a large number of cases. The detailed breakdown of this analysis can be found in Appendix B.

Another important observation we make is the difference in perturbation for different regions. As can be seen, not all regions are equally important when it comes to manipulating the prediction of a DNN with adversarial perturbation. We clearly observe adversarial perturbation applied to the center square being more influential than perturbation in other regions. Surprisingly, applying perturbation to randomly selected pixels requires less distortion than applying it to the frame of an image, further highlighting the differences between *important* and *unimportant* regions. Allowing perturbation in a more condensed area versus a more expanded area provides different results for the center square region and the other two regions. Increasing the number of selected pixels in the center square region also increases the $L_2$ norm of the perturbation, while doing so for frame and random pixels reduces the aforementioned norm.

## 5. Conclusion and Future Directions

We have proposed a simple and general method for localizing perturbations generated by existing adversarial attacks to specific image regions. Our method is experimentally confirmed to be effective, maintaining high black-box transferability at distortion levels that are significantly lower than the distortion levels required by existing attacks. The reduction in the amount of perturbation achieved by our method raises the concern that existing adversarial defenses may be undermined, since these are usually designed to be effective only against non-local attacks requiring larger perturbation budgets.

Our main priority for future work is (1) to investigate to what extent our localization method can fool state-of-the-art adversarial defenses as well as (2) to more precisely identify regions of importance where this localized perturbation can be made more effective, linking the observations made in this study to the interpretability of DNNs.

## References


Andriushchenko, M. and Hein, M. Provably Robust Boosted Decision Stumps and Trees Against Adversarial Attacks. In *Advances in Neural Information Processing Systems*, pp. 12997–13008, 2019.

Athalye, A., Carlini, N., and Wagner, D. Obfuscated Gradients Give A False Sense Of Security: Circumventing Defenses To Adversarial Examples. *CoRR*, abs/1802.00420, 2018.

Carlini, N. and Wagner, D. A. Towards Evaluating The Robustness of Neural Networks. *CoRR*, abs/1608.04644, 2016.

Carlini, N. and Wagner, D. A. Adversarial Examples Are Not Easily Detected: Bypassing Ten Detection Methods. *CoRR*, abs/1705.07263, 2017.

Cheng, S., Dong, Y., Pang, T., Su, H., and Zhu, J. Improving Black-box Adversarial Attacks with a Transfer-based Prior. In *Advances in Neural Information Processing Systems*, pp. 10932–10942, 2019.

Croce, F., Andriushchenko, M., and Hein, M. Provable Robustness of ReLU Networks via Maximization of Linear Regions. *CoRR*, abs/1810.07481, 2018.

Ghiasi, A., Shafahi, A., and Goldstein, T. Breaking Certified Defenses: Semantic Adversarial Examples with Spoofed Robustness Certificates. *CoRR*, abs/2003.08937, 2020.

Ghorbani, A., Abid, A., and Zou, J. Interpretation Of Neural Networks Is Fragile. *CoRR*, abs/1710.10547, 2017.

Goodfellow, I., Shlens, J., and Szegedy, C. Explaining and Harnessing Adversarial Examples. *CoRR*, abs/1412.6572, 2014.

Hara, K., Kataoka, H., and Satoh, Y. Can Spatiotemporal 3d CNNs Retrace the History of 2d CNNs and ImageNet? In *Proceedings of the IEEE conference on Computer Vision and Pattern Recognition*, pp. 6546–6555, 2018.

He, K., Zhang, X., Ren, S., and Sun, J. Deep Residual Learning For Image Recognition. In *Proceedings of the IEEE conference on computer vision and pattern recognition*, pp. 770–778, 2016.

Ilyas, A., Santurkar, S., Tsipras, D., Engstrom, L., Tran, B., and Madry, A. Adversarial Examples Are Not Bugs, They Are Features. In *Advances in Neural Information Processing Systems*, pp. 125–136, 2019.

Karmon, D., Zoran, D., and Goldberg, Y. Lavan: Localized and Visible Adversarial Noise. *CoRR*, abs/1801.02608, 2018.

Kindermans, P.-J., Hooker, S., Adebayo, J., Alber, M., Schütt, K. T., Dähne, S., Erhan, D., and Kim, B. The (Un) Reliability Of Saliency Methods. *CoRR*, abs/1711.00867, 2017.

Krizhevsky, A. and Hinton, G. Learning Multiple Layers Of Features From Tiny Images. Technical report, Citeseer, 2009.

Krizhevsky, A., Sutskever, I., and Hinton, G. E. Imagenet classification with deep convolutional neural networks. In *Advances in neural information processing systems*, pp. 1097–1105, 2012.

Kurakin, A., Goodfellow, I., and Bengio, S. Adversarial Examples In The Physical World. *CoRR*, abs/1607.02533, 2016.

LeCun, Y., Bottou, L., Bengio, Y., and Haffner, P. Gradient-Based Learning Applied To Document Recognition. *Proceedings of the IEEE*, 86(11):2278–2324, 1998.

Lowe, D. G. Distinctive Image Features from Scale-invariant Keypoints. *International journal of computer vision*, 60(2):91–110, 2004.

Madry, A., Makelov, A., Schmidt, L., Tsipras, D., and Vladu, A. Towards Deep Learning Models Resistant To Adversarial Attacks. *CoRR*, abs/1706.06083, 2017.

Moravec, H. P. Rover visual obstacle avoidance. In *Proceedings of the 7th International Joint Conference on Artificial Intelligence - Volume 2*, IJCAI81, pp. 785790, San Francisco, CA, USA, 1981. Morgan Kaufmann Publishers Inc.

Ozbulak, U., Van Messem, A., and De Neve, W. Impact Of Adversarial Examples On Deep Learning Models For Biomedical Image Segmentation. In *International Conference on Medical Image Computing and Computer-Assisted Intervention*, pp. 300–308. Springer, 2019.

Papernot, N., McDaniel, P. D., Jha, S., Fredrikson, M., Celik, Z. B., and Swami, A. The Limitations Of Deep Learning In Adversarial Settings. *CoRR*, abs/1511.07528, 2015.

Papernot, N., McDaniel, P. D., and Goodfellow, I. Transferability In Machine Learning: From Phenomena To Black-Box Attacks using Adversarial Samples. *CoRR*, abs/1605.07277, 2016.

Russakovsky, O., Deng, J., Su, H., Krause, J., Satheesh, S., Ma, S., Huang, Z., Karpathy, A., Khosla, A., Bernstein, M., Berg, A. C., and Fei-Fei, L. ImageNet Large Scale Visual Recognition Challenge. *International Journal of Computer Vision*, 115(3):211–252, 2015.

Schmid, C. and Mohr, R. Local Grayvalue Invariants for Image Retrieval. *IEEE transactions on pattern analysis and machine intelligence*, 19(5):530–535, 1997.

Schmidt, L., Santurkar, S., Tsipras, D., Talwar, K., and Madry, A. Adversarially Robust Generalization Requires More Data. In *Advances in Neural Information Processing Systems*, pp. 5014–5026, 2018.

Selvaraju, R. R., Das, A., Vedantam, R., Cogswell, M., Parikh, D., and Batra, D. Grad-Cam: Why Did You Say That? Visual Explanations From Deep Networks Via Gradient-Based Localization. *CVPR 2016*, 2016.

Simonyan, K. and Zisserman, A. Very Deep Convolutional Networks For Large-Scale Image Recognition. *CoRR*, abs/1409.1556, 2014.

Springenberg, J. T., Dosovitskiy, A., Brox, T., and Riedmiller, M. Striving For Simplicity: The All Convolutional Net. *CoRR*, abs/1412.6806, 2014.

Su, D., Zhang, H., Chen, H., Yi, J., Chen, P.-Y., and Gao, Y. Is Robustness the Cost of Accuracy?–A Comprehensive Study on the Robustness of 18 Deep Image Classification Models. In *Proceedings of the European Conference on Computer Vision (ECCV)*, pp. 631–648, 2018.

Su, J., Vargas, D. V., and Sakurai, K. One Pixel Attack For Fooling Deep Neural Networks. *CoRR*, abs/1710.08864, 2017.

Sun, Y., Wang, X., and Tang, X. Deep Learning Face Representation from Predicting 10,000 Classes. In *Proceedings of the IEEE conference on computer vision and pattern recognition*, pp. 1891–1898, 2014.

Szegedy, C., Zaremba, W., Sutskever, I., Bruna, J., Erhan, D., Goodfellow, I., and Fergus, R. Intriguing Properties Of Neural Networks. *CoRR*, abs/1312.6199, 2013.

Wong, E. and Kolter, J. Z. Provable Defenses Against Adversarial Examples via the Convex Outer Adversarial Polytope. *CoRR*, abs/1711.00851, 2017.

Xie, S., Girshick, R., Dollár, P., Tu, Z., and He, K. Aggregated Residual Transformations for Deep Neural Networks. In *Proceedings of the IEEE conference on computer vision and pattern recognition*, pp. 1492–1500, 2017.

Xu, K., Liu, S., Zhao, P., Chen, P.-Y., Zhang, H., Fan, Q., Erdogmus, D., Wang, Y., and Lin, X. Structured adversarial attack: Towards general implementation and better interpretability. *CoRR*, abs/1808.01664, 2018.

Zajac, M., Zołna, K., Rostamzadeh, N., and Pinheiro, P. O. Adversarial framing for image and video classification. In *Proceedings of the AAAI Conference on Artificial Intelligence*, volume 33, pp. 10077–10078, 2019.

# A. Experimental Details

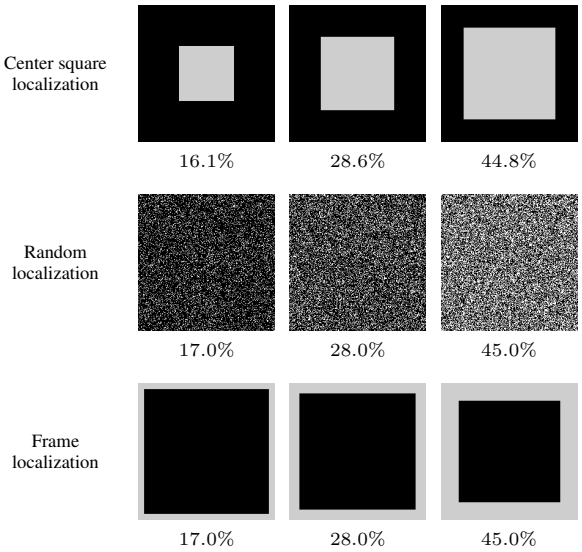


*Figure 3.* The localization masks used in this study. The given percentages correspond to the number of selected pixels compared to the total number of available pixels.

**Perturbation regions** In Figure 3, we provide visualizations of the selected localization masks, where the given percentages correspond to the proportion of selected pixels out of all available pixels.

Note that for the perturbation localized on the image frame, unlike Zajac et al. (2019), we do not expand the size of the image. We simply exercise the perturbation on the selected outermost pixels.

**Calculating $L_p$ distances** Between initial images of size $224 \times 224$ and their adversarial counterparts, we calculate $L_0$, $L_2$, and $L_\infty$ distances as follows:

$$L_0(\boldsymbol{X}, \tilde{\boldsymbol{X}}) = \frac{\sum_i^{224} \sum_j^{224} \mathbb{1}_{\{\boldsymbol{X}_{i,j} - \tilde{\boldsymbol{X}}_{i,j} \neq 0\}}}{224 \times 224}, \quad (4)$$

$$L_2(\boldsymbol{X}, \tilde{\boldsymbol{X}}) = ||\boldsymbol{X} - \tilde{\boldsymbol{X}}||_2, \quad (5)$$

$$L_\infty(\boldsymbol{X}, \tilde{\boldsymbol{X}}) = \max(|\boldsymbol{X} - \tilde{\boldsymbol{X}}|), \quad (6)$$

where $\boldsymbol{X}$ and $\tilde{\boldsymbol{X}}$ represent an initial image and its adversarial counterpart, respectively. In this framework, an $L_\infty$ norm of 1 means, added perturbation has changed a pixel from black to white (i.e., 0 to 255), or vice versa. An $L_0$ norm of 1 means all pixels are modified with the adversarial perturbation.

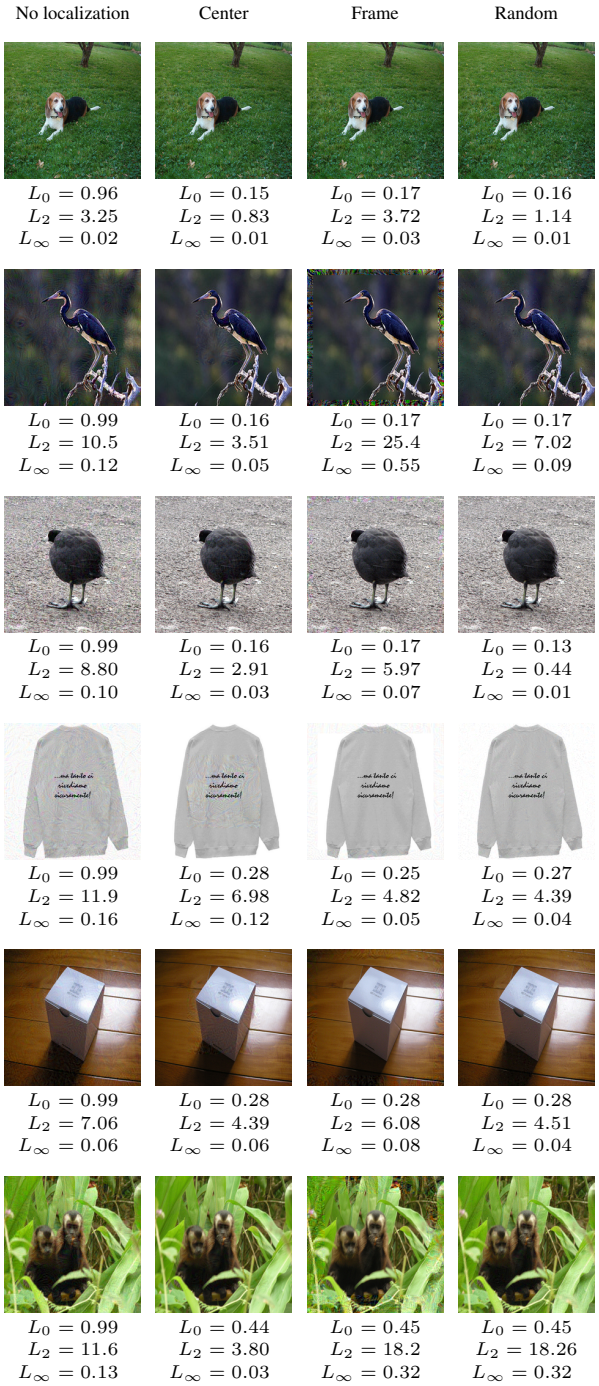


*Figure 4.* $L_0$, $L_2$, and $L_\infty$ distances between the initial images and their adversarial counterparts for the adversarial examples that originate from the same initial image but that were perturbed using different localization methods. All of the adversarial examples successfully transfer to models they are not originated from.

Target Model

| Source Model | AlexNet | VGG-16 | ResNet-50 |
|---|---|---|---|
| AlexNet | — | 99% | 99% |
| VGG-16 | 99% | — | 99% |
| ResNet-50 | 99% | 99% | — |

(a) 17% of pixels selected

Target Model

| Source Model | AlexNet | VGG-16 | ResNet-50 |
|---|---|---|---|
| AlexNet | — | 99% | 99% |
| VGG-16 | 99% | — | 99% |
| ResNet-50 | 99% | 99% | — |

(b) 28% of pixels selected

Target Model

| Source Model | AlexNet | VGG-16 | ResNet-50 |
|---|---|---|---|
| AlexNet | — | 99% | 99% |
| VGG-16 | 99% | — | 99% |
| ResNet-50 | 99% | 99% | — |

(c) 45% of pixels selected

Target Model

| Source Model | AlexNet | VGG-16 | ResNet-50 |
|---|---|---|---|
| AlexNet | — | 77% | 81% |
| VGG-16 | 77% | — | 84% |
| ResNet-50 | 82% | 85% | — |

(a) 17% of pixels selected

Target Model

| Source Model | AlexNet | VGG-16 | ResNet-50 |
|---|---|---|---|
| AlexNet | — | 80% | 76% |
| VGG-16 | 78% | — | 79% |
| ResNet-50 | 80% | 79% | — |

(b) 28% of pixels selected

Target Model

| Source Model | AlexNet | VGG-16 | ResNet-50 |
|---|---|---|---|
| AlexNet | — | 80% | 74% |
| VGG-16 | 74% | — | 68% |
| ResNet-50 | 77% | 76% | — |

(c) 45% of pixels selected

Target Model

| Source Model | AlexNet | VGG-16 | ResNet-50 |
|---|---|---|---|
| AlexNet | — | 52% | 43% |
| VGG-16 | 28% | — | 41% |
| ResNet-50 | 32% | 40% | — |

(a) 17% of pixels selected

Target Model

| Source Model | AlexNet | VGG-16 | ResNet-50 |
|---|---|---|---|
| AlexNet | — | 49% | 47% |
| VGG-16 | 34% | — | 49% |
| ResNet-50 | 28% | 49% | — |

(b) 28% of pixels selected

Target Model

| Source Model | AlexNet | VGG-16 | ResNet-50 |
|---|---|---|---|
| AlexNet | — | 62% | 55% |
| VGG-16 | 34% | — | 50% |
| ResNet-50 | 34% | 45% | — |

(c) 45% of pixels selected

*Figure 5.* The percentage of adversarial examples with regional perturbation that have less perturbation in terms of $L_0$ norm (top), $L_2$ norm (middle), and $L_\infty$ norm (bottom) compared to their counterparts with "global" perturbation. Percentages are calculated based on the adversarial examples with localized perturbation that transfer from source model to target model.

## B. Additional Experimental Results

In Figure 4, we provide a number of qualitative examples, showing the $L_0$, $L_2$, and $L_\infty$ norms of adversarial perturbation generated using various localization settings. All of the examples presented in Figure 4 are generated using AlexNet and transfer to ResNet-50.

For the experiments discussed in the main paper, Figure 5 provides the percentage of adversarial examples that have lower $L_p$ norm than their counterparts generated with "global" perturbation. Our experiments show that regional perturbation almost always leads to lower $L_0$ norms compared to non-regional perturbation, whereas in the case of $L_2$ and $L_\infty$ norms, this depends on the initial image-target class combination.

For the sake of completeness, In Table 2 we provide the exhaustive details of $L_0$ norms of adversarial perturbations for the experiment described in the main paper. Since the perturbation region is what is controlled in this experiment, the resulting perturbations have much less $L_0$ deviation compared to $L_2$ or $L_\infty$.

*Table 2.* Mean (standard deviation) $L_0$ distances calculated between genuine images and their adversarial counterparts, with the adversarial counterparts created by localization of perturbation (see the first column). Adversarial examples are created from the source models listed in the first row and transfer to the target models listed in the second row.

| Localization | Source: | AlexNet | | VGG-16 | | ResNet-50 | |
|---|---|---|---|---|---|---|---|
| | Target: | VGG-16 | ResNet-50 | AlexNet | ResNet-50 | AlexNet | VGG-16 |
| | Norm: | $L_0$ | | $L_0$ | | $L_0$ | |
| No Localization | | 0.93 (0.08) | 0.94 (0.07) | 0.90 (0.07) | 0.84 (0.11) | 0.89 (0.10) | 0.83 (0.10) |
| Center | 90px | 0.15 (0.01) | 0.15 (0.01) | 0.15 (0.01) | 0.15 (0.01) | 0.15 (0.01) | 0.14 (0.01) |
| | 120px | 0.27 (0.01) | 0.28 (0.01) | 0.27 (0.01) | 0.26 (0.03) | 0.27 (0.01) | 0.26 (0.03) |
| | 150px | 0.43 (0.02) | 0.43 (0.02) | 0.43 (0.02) | 0.40 (0.04) | 0.43 (0.02) | 0.41 (0.04) |
| Frame | 20px | 0.16 (0.01) | 0.16 (0.01) | 0.16 (0.01) | 0.16 (0.01) | 0.16 (0.01) | 0.16 (0.01) |
| | 34px | 0.27 (0.01) | 0.27 (0.01) | 0.27 (0.01) | 0.26 (0.02) | 0.27 (0.01) | 0.26 (0.02) |
| | 58px | 0.43 (0.02) | 0.43 (0.02) | 0.43 (0.02) | 0.42 (0.04) | 0.43 (0.04) | 0.42 (0.03) |
| Random | 17% | 0.16 (0.01) | 0.16 (0.01) | 0.16 (0.01) | 0.16 (0.01) | 0.16 (0.01) | 0.15 (0.01) |
| | 28% | 0.28 (0.01) | 0.28 (0.01) | 0.28 (0.01) | 0.27 (0.02) | 0.28 (0.01) | 0.27 (0.02) |
| | 45% | 0.44 (4.80) | 0.43 (0.11) | 0.43 (4.20) | 0.41 (0.09) | 0.43 (3.98) | 0.41 (0.09) |